Research on Fault Signal Reconstruction of Treadmill Equipment Based on Deep Neural Network

Lingling Cui[1(✉)] and Juan Li[2]

[1] Department of Physical and Health Education, Wuxi Vocational Institute of Commerce, Wuxi 214153, China
cl_ilikemouse@163.com

[2] College of Intelligent Equipment and Automotive Engineering, Wuxi Vocational Institute of Commerce, Wuxi 214153, China

Abstract. There are a large number of noise components in the fault signals of treadmill equipment, which leads to increased difficulty in signal reconstruction. Therefore, a new method for reconstructing fault signals of treadmill equipment is proposed by introducing deep neural networks. Based on the community structure, fault source localization is achieved through two stages: partitioning fault areas and predicting fault propagation paths. A fault signal acquisition platform is designed based on the fault source localization results, and the collection of fault signals from the treadmill equipment is implemented. A denoising model based on a dual-layer recurrent neural network is constructed using deep neural networks to perform denoising processing on the collected fault signals. The signal reconstruction of treadmill equipment faults is completed using a matching tracking algorithm. The test results show that the reconstruction time of this method is less than 6000 ms, and the minimum signal-to-noise ratio of the reconstructed signal reaches 49.30 dB, demonstrating good practical application effects.

Keywords: Deep Neural Network · Community Structure · Treadmill Equipment · Fault Signal Reconstruction · Orthogonal Matching Pursuit

1 Introduction

At present, busy work makes it difficult to regularly go to the gym for exercise, so exercising at home has become an increasing choice for people. As a kind of household fitness equipment, the Treadmill has obvious advantages that consumers can use the Treadmill to exercise enough even in their own narrow space. At the same time, it is convenient to install, simple to control, and can freely control the intensity and time of movement. Therefore, it has become a very popular sports equipment for consumers [2]. However, under frequent startup, shutdown, and speed regulation modes, the stator and rotor winding circuits of asynchronous motors are prone to generate huge heat, which can lead to thermal aging if they cannot dissipate heat in a timely manner. As a result, the

L. Yun et al. (Eds.): ADHIP 2023, LNICST 547, pp. 239–254, 2024.
https://doi.org/10.1007/978-3-031-50543-0_17

performance of asynchronous motors decreases sharply and faults are prone to occur. Therefore, fault signal reconstruction can improve the accuracy and efficiency of fault diagnosis.

In this context, scholars have conducted certain research work on fault signal reconstruction. So far, fault signal reconstruction methods mainly include methods based on multivariate statistical analysis, observer based methods, and machine learning methods. Among them, some scholars proposed a motor fault signal reconstruction method based on dyadic wavelet transform and triangular Spline interpolation. This method uses the same function - triangular spline wavelet function in dyadic wavelet transform and interpolation reconstruction, which can reflect the essence of signal processing. The proposed triangular spline wavelet has the dual function of serving as both a wavelet function and an interpolation function, greatly improving the effectiveness of the algorithm. It was applied to the reconstruction process of motor fault signals and compared with the Mallat algorithm in terms of signal-to-noise ratio and relative error, with significant results. Some scholars have proposed a multi-sensor rolling bearing fault signal reconstruction method based on the correlation principle. In order to compensate for the defect of incomplete signal collection by a single sensor, a multi sensor array is used to non-contact collect the periodic signal of rolling bearing faults and eliminate excess information. The correlation algorithm is used to reconstruct the incomplete signal fragments into a complete periodic acoustic signal of rolling bearing faults. And a calculation example of multi-sensor waveform data reconstruction is provided to verify the effectiveness of this method. The problems of long reconstruction time and low signal-to-noise ratio of reconstruction signal existing in the above methods are taken as research objectives, and a fault signal reconstruction method of Treadmill equipment based on deep neural network is designed.

2 Design of Fault Signal Reconstruction Method for Treadmill Equipment

2.1 Fault Source Location

Based on the community structure, fault source localization is achieved through two stages: dividing fault areas, predicting fault propagation paths, and locating fault sources. Design a fault source localization method based on the community structure. When a community node is detected to be in a fault state, it cannot be directly determined that the node has malfunctioned. The fault may also be caused by adjacent, highly capable fault nodes through fault propagation. Therefore, a retrospective approach is adopted to achieve fault source localization. At the same time, in order to quickly traverse the fault path, depth first traversal is used for path search [4].

The fault location process is divided into two stages: Dividing the fault area and predicting the fault propagation path to locate the fault source.

(1) Division of fault area

This stage is responsible for obtaining fault set α from the system that detected the fault, thereby dividing the network β where the fault alarm occurred into normal area χ

and fault area α, namely:

$$\chi \cup \alpha = \beta \tag{1}$$

The depth first traversal search and backtracking technology is mainly used for fault area division. The specific process is as follows:

Step 1: Initialize the fault set. Add the detected faulty node to α, randomly select a node from the fault set and start a reverse radial search to determine whether the node has been searched. If not, set it as starting node W and mark it; Otherwise, reselect a node that has not been searched for, set it as the starting node, and mark it as [5].

Step 2: Searches for the fault propagation path. Use depth first traversal and backtracking techniques for reverse search to determine the possible propagation path and corresponding node set of the node fault. Search for nodes with fault propagation impact on the current node, assuming E nodes, and determine whether E node has been searched. If node E is not searched, add that node to the fault propagation path set $H(W)$, record the propagation path, and mark that node as searched.

Step 3: Determines whether the backtracking condition is met. Repeat Step 2 until there is no fault propagation trend at node E. If it has been searched, it is determined that all nodes affected by the fault have been searched; On the contrary, search for other propagation paths and corresponding nodes. If both the path and the node have search marks, it will be traced back to the previous node.

Step 4: Determine whether to end the current search. Repeat Step 3 until the start node is traced back, and judge whether the nodes connected to it have search marks. If not, start searching again from the node that has not been searched; If yes, the affected fault set search for the failed node has been completed.

Step 5: Determine whether to end the fault area division. Determine whether all nodes in α have been searched. If not, set one of the nodes as the starting node W and return to step 2; If all faulty nodes are searched, add the intersection of the fault propagation path sets of each node to α, and the fault area division ends [6].

(2) Predict propagation path and locate fault source

After determining the fault area α, analyze the structural characteristics of the area, and the specific fault source localization process can be divided into the following steps:

Step 1: Determine the size of the fault area. For fault area α, first determine the following equation:

$$|\alpha| = 1 \tag{2}$$

When the above formula is true, it indicates that there is only one fault source at present. Output the node to end the positioning; Otherwise, it indicates that there are multiple fault nodes. Enter Step 2.

Step 2: Determines whether there are independent subnets in α. If it exists, it indicates that multiple fault alarms have occurred in different regions. It is necessary to locate the fault source α of each independent sub network as the fault area and return to Step 1; Otherwise, store the nodes within α into the fault prediction set U and enter Step 3.

Step 3: Sort the nodes of the fault prediction set. Calculate the fault occurrence rate g_v for each node c_v in fault prediction set U, sort from high to low, and select the node with the highest fault occurrence rate as $c_{\max}$.

Step 4: Predicts the fault propagation path and locates the fault source. Calculate the fault occurrence rate of each path node in the fault propagation path set $H(c_{\max})$ of $c_{\max}$, comprehensively consider the impact of fault propagation on the path node and the historical changes in fault occurrence rate, determine whether the fault propagates between each node, and obtain the set K of fault propagation paths. Select the node that is most likely to fail in set K as the expected fault source node and store it in fault source set V.

Step 5: Outputs the results. If there are independent subnetworks in the fault area α of Step 2, the predicted fault source nodes found in all subnetworks will form the predicted fault source set V, and the corresponding propagation path will be recorded to complete fault localization and output the localization results.

2.2 Fault Signal Acquisition

The fault signal acquisition platform is designed based on the fault source location results, and the fault signal acquisition of Treadmill equipment is implemented. The platform selects Altera Cyclone IV FPGA as the control core. Firstly, after the acceleration sensor is assembled as required, the platform starts to collect the fault signal of the treadmill equipment. The collected signals are filtered and amplified by the signal conditioning module, and then converted into voltage signals and sent to the AD conversion module. FPGA is responsible for controlling AD chip to convert data, and then performing FIR filtering pretreatment on the converted digital signal. Then, control the two pieces of RAM to complete FIFO data cache in ping-pong structure and send it to SDRAM for real-time storage. It is connected to the upper computer through RS232 serial port or Ethernet, and the serial port and TCP protocol are used for data transmission. Finally, the control network interface chip transmits the data to the upper computer [7]. After the hardware system is connected to the server created by the upper computer, wait for the upper computer to receive data. The upper computer will carry out system analysis and data processing for these data respectively.

The selected sensor is an acceleration sensor. In view of the comprehensive consideration of various parameter ranges of the sensor and its installation environment and other factors, we have adopted the YK-YD20 acceleration sensor of IEPE type. The sensor has a built-in charge amplifier, which has the advantages of large dynamic range, wide frequency response, strong anti-interference ability, etc., and greatly suppresses the increase of noise. The parameters of YK-YD20 acceleration sensor are shown in Table 1.

In order to ensure the normal operation of IEPE type acceleration sensor YK-YD20, it is generally necessary to stimulate (2–20 mA) with a quantitative constant current source to output a constant current to effectively avoid damage to the sensor caused by excessive current. In order to achieve the effective output of constant current excitation, we have chosen LM334 chip for design after comprehensive consideration. Constant current source is greatly affected by temperature, and its output current will change with the difference of temperature factors. Therefore, it can be regarded as a constant current source only when it maintains constant temperature. In order to prevent the impact of temperature, it is necessary to add a resistor and diode on the original basis, which can effectively reduce the current drift [8] caused by temperature changes.

Table 1. YK-YD20 acceleration sensor parameters

S/N	Project	Parameter
1	Measuring range	100 g
2	Frequency range	0.2–5 kHz
3	Supply voltage	12 V–28 V (DC)
4	Maximum allowable acceleration	5 * 100 m·s-2
5	Sensitivity	50 mV/g
6	Working temperature	−50 °C− + 120 °C
7	Transverse sensitivity ratio	≤8%
8	Working current	1–10 mA

The operational amplifier designed with LM358 chip is a co directional proportional amplifier circuit. The two internal amplifiers have high gain and are independent of each other. Through sensor sensitivity PK, measured vibration acceleration a, and charge amplifier sensitivity AK, it can be calculated that the sensor output voltage is about 1 V. Since the input voltage of the AD chip used in the platform acquisition module is ±5 V, ensure that the sensor is normally connected to the AD conversion circuit and can only amplify the input signal.

This circuit is a typical voltage series negative feedback circuit. The acceleration sensor YK-YD20 outputs a voltage of v_q and is connected to the in-phase input terminal of the amplification circuit through a resistor. The amplified output voltage of v_p is connected to the inverting input terminal of the operational amplifier circuit using two resistors. Due to the negative feedback circuit of LM358 and its gain approaching 100 dB, it is considered a linear state. The two input terminals of the operational amplifier can be regarded as equal voltages, namely:

$$v_1 = v_2 \tag{3}$$

The input current is zero, that is, the definition of virtual short and virtual break. According to the resistance voltage division formula:

$$v_2 = \frac{R_a}{R_b + R_a} v_q \tag{4}$$

In Eq. (4), R_a and R_b are external resistors.

$$v_1 = \frac{R_c}{R_d + R_c} v_p \tag{5}$$

In Eq. (5), R_c and R_d are internal resistances. Due to the need to design an amplification circuit with a voltage amplification factor of 5, 5k resistors of R_c, R_d, and 1k resistors of R_a and R_b will be selected, and finally substituted into the above formula to calculate the ratio of v_q to v_p as 5.

FPGA is used as the control chip, mainly because it has rich I/O pin resources. It includes 8 user I/O blocks, and the number of I/Os available to users is 179, which makes it easier to achieve logical control. In this platform, FPGA is mainly responsible for the acquisition and processing of the signal module and the control of the signal transmission to the upper computer. When selecting FPGA, it is necessary to consider the low cost and low power FPGA architecture designed, and select according to the design requirements. Therefore, this paper selects the fourth generation Cyclone IV series FPGA devices produced by ALTERA Company, and selects EP4CE10F17C8 chip as the platform FPGA device chip [9].

According to the chip manual, EP4CE10F17C8 is powered by three different voltages. In order to meet the demand of the power circuit, the voltage conversion chip is used to convert 5 V voltage into different voltage values of 1.2 V/2.5 V/3.3 V, so as to ensure the normal operation of the FPGA control module. It is understood that 1.0 V/1.2 V voltage is required to be supplied to the internal logic voltage (VCCINT) and PLL digital voltage (VCCD_PLL), 2.5 V is required to supply PLL analog voltage (VCCA), and 3.3 V voltage is required to be supplied by IO for the rest.

Cyclone IV series FPGAs are configured in active serial (AS), passive serial (PS), JTAG, etc. FPGA device adopts SRAM architecture, which belongs to volatile memory architecture. Therefore, nonvolatile memory chips must be added to the platform. The 16Mbit nonvolatile memory chip EPCS16 designed by Altera Company was selected. Configure the pins in the Table 2 below for the chip.

Table 2. Function table of configured circuit pins

S/N	Pin name	Function
1	ASDI	Data writing
2	nCS	Chip Select
3	DCLK	Clock signal input
4	DATA	data output

AD acquisition circuit controls the reception of signals, and converts the received analog signals into data signals for the analysis and processing of upper computer data. Because the A/D conversion module has complex performance, when designing the hardware of the A/D module, all the pins on the chip are connected to the FPGA. Through the design of the logical A/D conversion module, the corresponding functions are controlled and realized. This paper uses the AD7606 A/D conversion chip designed and produced by an American company. The chip can support 16 bit synchronous sampling, with a sampling rate of up to 200K, and also has the characteristics of 40 dB anti aliasing suppression signal.

The data conversion of AD7606 chip is controlled by two pins CONVST A and CONVST B, so connecting CONVST A and CONVST B can effectively complete eight channel synchronous sampling. Among them, CONVST A controls the four channels V1–V4, while the other pin controls the remaining four channels.

The memory selected is W9812G6KH-75 as the cache chip. The maximum clock of this chip can reach 133 MHz, and data reading and writing can be completed in a short time. Moreover, the memory capacity of the chip is 4 Banks * 1 Mbits * 16, or 64 Mbit, which largely meets the data storage requirements of the platform.

The selected UART device is RS232 interface, which is mainly used for the communication between the data acquisition module and the PC, and RS232 can also complete two-way data transmission and full duplex communication, so it is widely used in short distance data transmission. Since the input and output of FPGA pin is TTL level, the platform uses serial port conversion core MAX3232 that supports RS232 protocol for data conversion.

W5300 chip is selected to realize the network data upload function. W5300 chip supports TCP/IP protocol stack. The processor only needs to set network parameters such as IP address and mask to perform TCP/IP connection. Its advantage is not only fast, stable and reliable, but also effectively saves the ROM resources of the processor. Connect W5300 to FPGA through the connection mode of control pin. See Table 3 for details.

Table 3. Control pin and function

S/N	Pin	Function description
1	OP_Mode[2:0]	Operation mode selection of internal PHY chip
2	TestMode[3:0	PHY chip mode selection
3	RD	Read enable signal
4	WR	Write enable signal
5	CS	Chip select
6	DATA[15:0]	Data bus signal
7	ADDR9	Address bus signal
8	BIT16EN	Data bit selection
9	RESET	Hardware reset signal input

RJ45 Ethernet interface is adopted, and HX1188 is selected as Ethernet isolation transformer.

2.3 Signal Noise Reduction Processing

Based on the deep neural network, a noise reduction model of a two-layer recurrent neural network is constructed to denoise the collected fault signals [10]. In the input layer, the data set is divided, and the ratio of test set and training set is 7:3. Define the input data as:

$$Y = \{y_1, y_2, \ldots, y_m\} \tag{6}$$

In formula (6), m represents the input data length.

Predict the next fault data 45 based on the fault data $\{y_1, y_2, \ldots, y_{100}\}$ of the first y_{101} moments of the asynchronous motor. Then use $\{y_1, y_2, \ldots, y_{101}\}$ data to predict y_{102}, and so on [11]. The entire model framework consists of four parts, and the network model has four layers. The input layer is responsible for formatting the data, and the output layer is used to output noise reduction results. In order to prevent overfitting, the hidden layer is built with LSTM-GRU and double-layer LSTM, and connected through the Dropout layer [12].

When the neural network unit core is at time t, it receives xtof the current state and output ht – 1 of the hidden layer state of the previous time (t − 1) as the input of the entire neural network unit, which is combined with the weight and bias of the input gate, output gate and forgetting gate respectively to obtain the signal values of the input gate, output gate and forgetting gate. Then update the memory cell c and the current time ht according to the current signal, and use them as the input of the next layer of neural network core unit [13].

In the process of noise reduction for error data, the selection of model parameters determines the quality of network performance and the accuracy of noise reduction results. In this model, there are two main types of parameters. One is the parameters automatically updated and learned through the network model in the training process, and its settings are shown in Table 4.

Table 4. Model parameter settings

S/N	Model parameter	Parameter setting
1	Neuron inactivation ratio dropout	0.1
2	Optimization algorithm	Dropout layer import
3	Initial learning rate	0.005
4	Number of batches	30
5	Number of hidden layers	2
6	Output layer node	1
7	Number of hidden layer nodes	8
8	time step	100

The other is the setting of super parameters, such as learning rate, iterations, and loss function selection.

(1) Super parameter setting

The mean square error in the network model is taken as the loss function, and the mean square error formula is as follows:

$$MSE = \frac{1}{M}\sum_{j=1}^{M}\left(\bar{s}_j - h_j\right)^2 \tag{7}$$

In the above equation, M represents the number of samples used in the iteration; $\overline{s}_j$ represents the j-th data denoising value; h_j represents the original drift error of the j-th data.

(2) Weight parameter update

After the super parameters are set, the double-layer network model learns the error data characteristics through the training of the sample set. The Adam algorithm is used to continuously update the weight and adjust the weight parameters through back propagation. When the loss function is not decreasing or the whole training process is over, the weight and offset are saved. The noise reduction model reduces the noise of data at the next time through the weight and deviation of training.

The Adam algorithm execution flow chart is shown in Fig. 1.

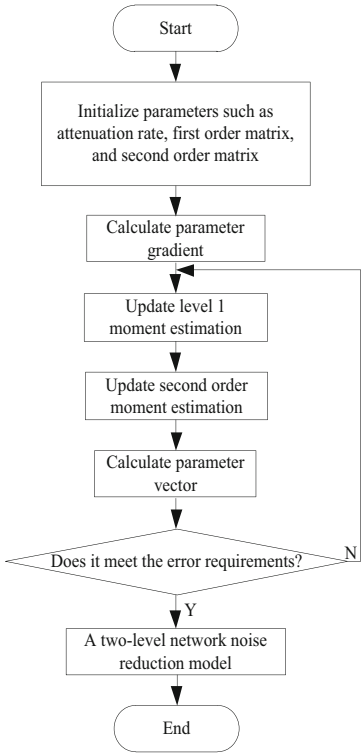

Fig. 1. Adam algorithm execution flow chart

The noise reduction of fault signal is completed through this model.

2.4 Signal Reconstruction

Based on the signal after noise reduction, the signal reconstruction of Treadmill equipment fault is completed by using Matching pursuit algorithm. The regularized orthogonal matching pursuit algorithm of the compressed sensing reconstruction algorithm is an improvement on the orthogonal matching pursuit algorithm [14]. In each iteration, the orthogonal matching pursuit algorithm will only select the column most related to the residual, but it is problematic to select only one column. To solve this problem, a regularized orthogonal matching pursuit is proposed.

Basic symbol description: ω is the original signal, which is ξ dimensions, and ψ is the observation vector, which is ζ dimensions. The general formula is established as follows:

$$\zeta < \xi \tag{8}$$

In reality, ω is generally not sparse, but in a certain transformation domain υ is sparse, that is:

$$\omega = \vartheta \upsilon \tag{9}$$

In formula (9), ϑ represents the sparse coefficient of O, which means that the absolute values of only O non zero terms or O element coefficients of ϑ are much greater than zero.

The observation vector in compressed observation satisfies the following equation:

$$\psi = \varpi \omega \tag{10}$$

In formula (10), ϖ represents an empty set.

In a certain transformation domain υ, the following equation holds:

$$\psi = \varpi \vartheta \upsilon \tag{11}$$

The following formula is established:

$$\varpi \upsilon = \mathrm{B} \tag{12}$$

The following formula is established:

$$\psi = B\vartheta \tag{13}$$

In the ROMP reconstruction algorithm, there are also the following symbols, as shown in Table 5.

Table 5. Other symbols

S/N	Symbol	Significance
1	t_r	Residual
2	r	Iterations
3	μ_r	Index found in r-th iteration
4	Δ_r	Index set for the r-th iteration
5	B_i	Column i of matrix B
6	ρ_r	Column vector of $r * 1$
7	B_r	Column set of matrix B selected by index μ_r

The ROMP reconstruction algorithm process is described in detail as follows:

(1) Input:
1. Sensing matrix $\mathrm{B} = \varpi\upsilon$ of $\zeta \times \xi$;
2. ξ*1-dimensional observation vector ψ;
3. Signal sparsity H.

(1) Firstly, initialize each quantity:

$$t_0 = \psi \tag{14}$$

In formula (14), t_0 represents the initial value of the residual.

$$\Delta_0 = \lambda \tag{15}$$

In formula (15), λ represents an initial value set; Δ_0 represents the initial value of Δ_r.

$$B_0 = \lambda \tag{16}$$

In formula (16), B_0 represents the initial value of B.

$$r = 1 \tag{17}$$

(2) Calculate $\langle t_{r-1}, B_i \rangle$, select the H maximum values or all non zero values in the result, and form a set I with column numbers i corresponding to B.

(3) Regularization: Find subset I_0 in set I, which satisfies the following formula:

$$\begin{cases} |R(I_1)| \leq |R(I_2)| \\ I_1, I_2 \in I_0 \end{cases} \tag{18}$$

Select the I_0 with the highest energy among all subsets I_0 that meet the requirements.

(4) The following formula is established:

$$\begin{cases} \Delta_r = \Delta_{r-1} \cup I_0 \\ B_r = B_{r-1} \cup B_i \\ i \in I_0 \end{cases} \tag{19}$$

(5) Find the least squares solution of $\psi = B_r \vartheta_r$.
(6) Update the residuals using the results from the previous step.
(7) Increase the number of iterations by one. If the number of iterations is less than or equal to H, return to step (2), otherwise proceed to the next step.
(8) The sparse representation coefficients of the reconstructed signal are estimated to have non-zero terms at Δ_r locations, with their values being the least squares solutions obtained from the last iteration [15].
(9) Output:
1. Estimation of signal sparse representation coefficient;
2. ξ * 1 dimensional residual

3 Signal Reconstruction Test

3.1 Experimental Process

For the designed method of fault signal reconstruction of treadmill equipment based on deep neural network, use it to reconstruct the fault signal of a treadmill equipment, and test the performance of the method. First, the fault source location method based on community structure is used to implement the fault location of the treadmill equipment, and then the fault signal acquisition platform is used to implement the fault signal acquisition. The collected fault signal is shown in Fig. 2.

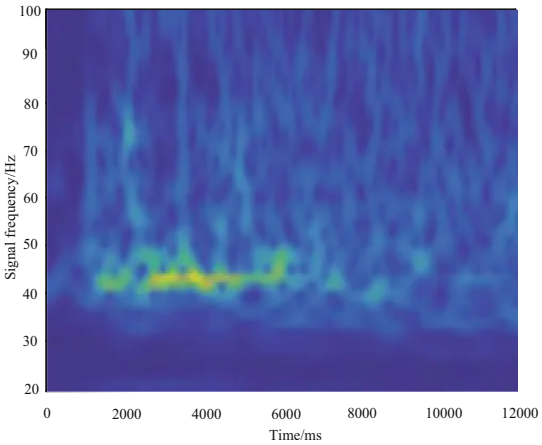

Fig. 2. Fault signal collected

The denoising model based on the two-layer recurrent neural network is used to implement the signal denoising. The signal after noise reduction is shown in Fig. 3.

Finally, the signal reconstruction of treadmill equipment fault is realized by matching pursuit algorithm. The reconstructed signal is shown in Fig. 4.

The time spent in testing the reconstructed signal and the signal-to-noise ratio of the reconstructed signal. In the test Motor fault signal reconstruction method based on dyadic wavelet transform and triangular spline interpolation. Compared with the reconstruction method of multi-sensor rolling bearing fault signal based on correlation principle, the method is tested together and represented by method 1 and method 2.

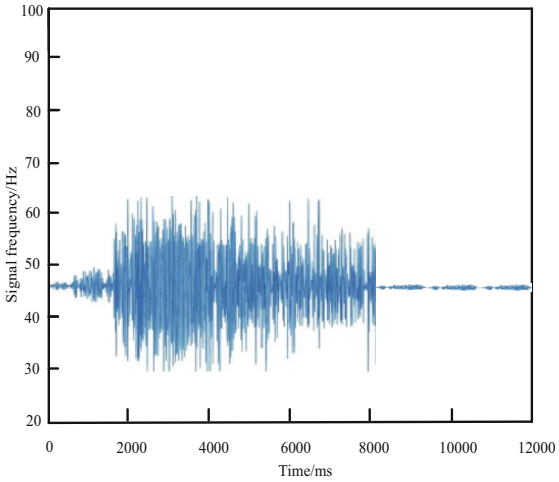

Fig. 3. Signal after noise reduction

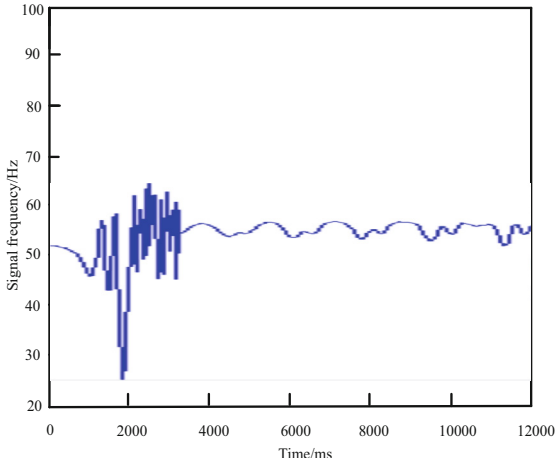

Fig. 4. Reconstructed signal

3.2 Reconstruction Time Test Results

The design method and the reconstruction time test results of method 1 and method 2 are shown in Fig. 5.

The reason is that this method constructs a noise reduction model based on the double-layer Recurrent neural network according to the deep neural network, realizes the noise reduction processing of the collected fault signal, and completes the signal reconstruction of treadmill equipment fault by combining the signal noise reduction processing results with the matching pursuit algorithm. Therefore, this method has lower reconstruction time and higher reconstruction efficiency.

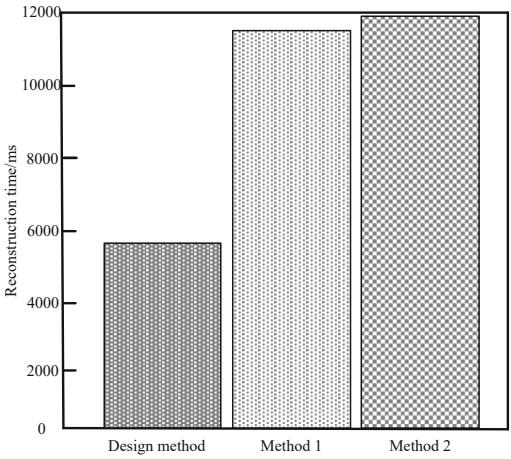

Fig. 5. Reconstruction time test results

3.3 Signal to Noise Ratio Test Results of Reconstructed Signal

The reconstructed signal SNR test results of the three methods are shown in Table 6.

Table 6. Signal to noise ratio of reconstructed signal of three methods

Iterations	Signal to noise ratio (dB)		
	Design method	Method 1	Method 2
5000	50.52	20.36	24.36
6000	50.30	20.01	24.18
7000	50.05	19.96	24.05
8000	49.92	19.64	23.94
9000	49.56	19.38	23.84
10000	49.30	18.97	23.64

According to the test results in the table above, the reconstructed signal signal-to-noise ratio of the design method reaches a minimum of 49.30 dB, while the signal-to-noise ratios of Method 1 and Method 2 are only 18.97 dB and 23.64 dB, respectively. The signal-to-noise ratio of the design method is lower. The signal to noise ratio of the reconstructed signal of the design method is up to 50.52 dB, while the signal to noise ratio of the method 1 and method 2 is only 20.36 dB and 23.64 dB. The reason is that the design method builds a noise reduction model based on the double-layer recurrent neural network according to the depth neural network to achieve the noise reduction of the collected fault signal, so the signal to noise ratio of the reconstructed signal of this method is always kept at a high level.

4 Conclusion

The fault signals of treadmill equipment contain a large amount of noise components, which increases the difficulty of signal reconstruction. Therefore, deep neural networks are introduced to design a new method for reconstructing fault signals of treadmill equipment. This method mainly involves constructing a denoising model based on a dual-layer recurrent neural network using deep neural networks, performing denoising processing on the collected fault signals, and completing the signal reconstruction of treadmill equipment faults using a matching tracking algorithm. The superiority and effectiveness of this method are highlighted through relevant comparative experiments. In summary, the reconstruction of fault signals in treadmill equipment not only improves fault diagnosis accuracy and maintenance efficiency but also promotes the development of intelligent maintenance technology. However, there are inherent limitations such as limited knowledge and insufficient research depth. Therefore, there are still many shortcomings in related research work that need to be further studied and optimized.

References

1. Wang, H., Cheng, Y., Tian, Z.: A new signal fault detection algorithm for vector tracking loop in strong noise environments. J. Northwest. Polytech. Univ. **40**(2), 323–329 (2022)
2. Jiang, J., Cong, X., Li, S., et al.: A hybrid signal-based fault diagnosis method for lithium-ion batteries in electric vehicles. IEEE Access **9**, 19175–19186 (2021)
3. Hu, H.Y., Wang, C., Liu, R.D., et al.: Speed sensorless control of induction motor based on stator current series model. Comput. Simul. **38**(04), 177–181 (2021)
4. Gao, F., Li, F., Wang, Z., et al.: Research on multilevel classification of high-speed railway signal equipment fault based on text mining. J. Electric. Comput. Eng. **2021**(2), 1–11 (2021)
5. Li, F., He, Z., Zhang, L., et al.: Analytical model and spectral characteristics of acoustic emission signal produced by localized fault of rolling element bearing. J. Northwest. Polytech. Univ. **39**(4), 831–838 (2021)
6. Teguia, J.B., Kammogne, A.S.T., Ganmene, S.G.T., et al.: Fuzzy-enhanced robust fault-tolerant control of IFOC motor with matched and mismatched disturbances. Math. Found. Comput. **5**(4), 295–314 (2022)
7. Shi, L., Zhu, Y., Zhang, Y., et al.: Fault diagnosis of signal equipment on the Lanzhou-Xinjiang high-speed railway using machine learning for natural language processing. Complexity **2021**(8), 1–13 (2021)
8. Ren, Z., Wu, G., Wu, Z., et al.: Hybrid dynamic optimal tracking control of hydraulic cylinder speed in injection molding industry process. J. Ind. Manag. Optim. **19**(7), 5209–5229 (2023)
9. Ives, Z.G.: Solving the signal reconstruction problem at scale: technical perspective. Commun. ACM. ACM **64**(2), 105 (2021)
10. Li, Z., Wu, H., Cheng, L., et al.: Infrared and visible fusion imaging via double-layer fusion denoising neural network. Digit. Sig. Process. **123**(1), 103433–103445 (2022)
11. Wen, Z., Wang, H., Gong, Y., et al.: Denoising convolutional neural network inspired via multi-layr convolutional sparse coding. J. Electron. Imaging **30**(2), 023007–023027 (2021)
12. Han, Z.: Nonlinear model predictive control of single-link flexible-joint robot using recurrent neural network and differential evolution optimization. Electronics **10**(19), 2426–2437 (2021)

13. Chen, C., Tian, Y., Gao, Q., et al.: Frequency-division abnormal amplitude attenuation after data reconstruction based on random function and its application in the very thick loess tableland area, ordos basin. Geophys. Prospect. Petrol. **58**(5), 741–749 (2022)
14. Han, C.: The analysis about compressed sensing reconstruction algorithm based on machine learning applied in interference multispectral images. Adv. Multimedia **21**(Pt.1), 1–6 (2021)
15. Polat, N., Kayhan, S.K.: FPGA implementation of LSD-OMP for real-time ECG signal reconstruction. Turk. J. Electr. Eng. Comput. Sci. **29**(4), 1887–1907 (2021)